Learning Optimal Parametric Hydrodynamic Database for Vortex-Induced Crossflow Vibration Prediction of Both Freely-Mounted Rigid and Flexible Cylinders

Samuel Rudy [a], Dixia Fan [a,b], Jose del Aguila Ferrandis [a], Themistoklis Sapsis [a] and Michael S. Triantafyllou [a]
[a] Department of Mechanical Engineering, Massachusetts Institute of Technology, Cambridge, MA 02139, USA
[b] Department of Mechanical and Material Engineering, Queen's University, Kingston, Ontario, K7M 3N9, Canada

ABSTRACT

The Vortex-induced vibration (VIV) prediction of long flexible cylindrical structures relies on the accuracy of the hydrodynamic database constructed via rigid cylinder forced vibration experiments. However, to create a comprehensive hydrodynamic database with tens of input parameters including vibration amplitudes and frequencies and Reynolds number, surface roughness and so forth is technically challenging and virtually impossible due to the large number of experiments required. The current work presents an alternative approach to approximate the crossflow (CF) hydrodynamic coefficient database in a carefully chosen parameterized form. The learning of the parameters is posed as a constraint optimization, where the objective function is constructed based on the error between the experimental response and theoretical prediction assuming energy balance between fluid and structure. Such a method yields the optimal estimation of the CF parametric hydrodynamic database and produces the VIV response prediction based on the updated hydrodynamic database. The method then was tested on several experiments, including freely-mounted rigid cylinder in large Reynolds number with combined crossflow and inline vibrations and large-scale flexible cylinder test in the Norwegian Deepwater Program, and the result is shown to robustly and significantly reduce the error in predicting cylinder VIVs.

KEY WORDS: VIV; Marine Risers; Hydrodynamic Database; Optimization; Digital Twin.

INTRODUCTION

The prediction of the bluff body vortex-induced vibrations (VIV) is a challenging but important problem. For example, if the VIV of a marine riser in the ocean current is not treated appropriately, it may result in severe fatigue damage and substantial economic and environmental loss. Therefore, due to its critical scientific and industrial applications, VIV has received a considerable amount of research attention in the last four decades. A large number of publications (Williamson *et al*, 2004; Gabbai *et al*, 2005; Wang *et al*, 2020) have reviewed the key concepts and principal mechanisms of the bluff body VIV's response and its wake patterns.

One of the major difficulties in modeling and predicting the VIV of bluff body structures relies on the accuracy of the hydrodynamic force on the rigid cylinder and its distribution along the span of the flexible model (Fan *et al*, 2017; Fan *et al*, 2019(1); Wang, *et al*, 2021). The fluid force on oscillating cylinders varies significantly as a function of structural and flow properties (Williamson *et al*, 1996; Xu *et al*, 2013; Chen *et al*, 2013). Therefore, to quantitatively study the fluid forces on oscillating cylinders in the current, experiments were conducted, where a rigid cylinder is forced to vibrate with prescribed trajectories (Gopalkrishnan *et al*, 1993; Aronsen *et al*, 2007; Dahl *et al*, 2008; Fan *et al*, 2019(2)). Especially for the CF vibration, the study focuses on the lift coefficient in-phase with the velocity C_{lv}, and the added mass coefficient in the CF direction C_{my} as a function of true reduced frequency $f_r = \frac{fD}{U}$ and non-dimensional CF amplitude $A^* = \frac{A_y}{D}$, where U is the prescribed fluid velocity, f is the prescribed motion frequency, A_y is the prescribed motion amplitude and D is the cylinder diameter.

The measured hydrodynamic coefficients are not only helpful in understanding the nature of the rigid cylinder free vibration but also serve as the fluid force database of several semi-empirical codes (Triantafyllou *et al*, 1999; Roveri *et al*, 2001; Larsen *et al*, 2001) for flexible riser response in the ocean current, assuming that the strip theory is valid (Han *et al*, 2018; Fan *et al*, 2019(1); Wang *et al*, 2021). However, to create a comprehensive hydrodynamic database with tens of input parameters including vibration amplitudes and frequencies as well as Reynolds number Re (Xu *et al*, 2013), surface roughness (Chang *et al*, 2011), riser configurations (Lin *et al*, 2020) and so forth is technically challenging and virtually impossible due to the large number of experiments required. Besides, during the lifetime of a riser in the field, long-term effects, such as equipment aging and bio-fouling, inevitably alter the hydrodynamic coefficients, making long-term riser prediction and monitoring even more challenging.

Therefore, the current work presents an alternative approach to approximate the crossflow (CF) hydrodynamic coefficient database in a carefully chosen parameterized form. The learning of the parameters is posed as a constraint optimization, where the objective function is constructed based on the error between the experimental response and theoretical prediction assuming energy balance between fluid and structure. Such a method yields the optimal estimation of the CF parametric hydrodynamic database and produces the VIV response prediction based on the updated hydrodynamic database. The method then was tested on a freely-mounted CF-only vibrating rigid cylinder in a moderate Re and a large-scale flexible cylinder test in the Norwegian Deepwater Program, and the result is shown to robustly and significantly reduce the error in predicting cylinder VIVs.

MATERIALS AND METHODS

Hydrodynamic Parameterization

Shown in Fig. 1, many of the desired properties of C_{lv} and C_{my} may be captured in a simple piecewise linear model: for example, the region of positive C_{lv} is associate with particular A^* and f_r regions; C_{my} is found to abruptly change from the small negative value to a large positive value at given f_r and is weakly dependent on A^*. The above characters are given in a parameterized form quantified by parameters p_i to be learned from the data.

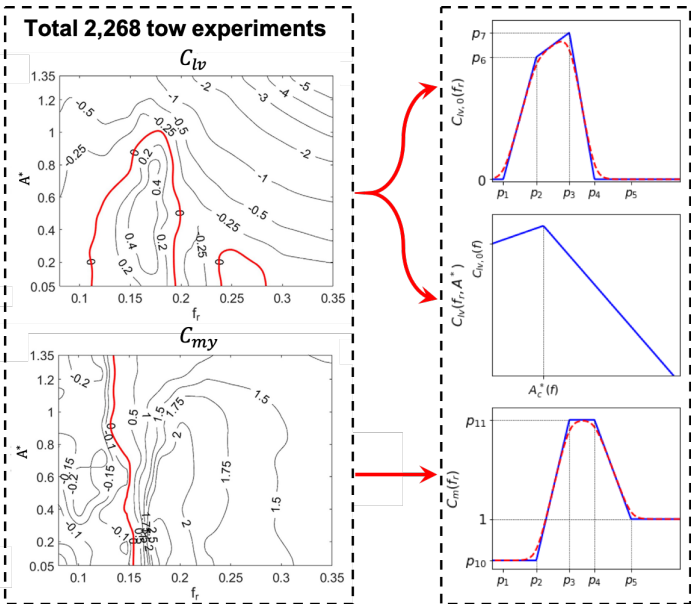

Fig. 1 The simplification of a hydrodynamic coefficient database constructed by a large number of rigid forced vibration experiments (left) (Fan *et al*, 2019(2)), using simple piecewise linear models with a set of parameters to be learned from the data (right).

In this work, we use a smoothed variation of the model shown in Fig. 1 to parameterize functional forms for the unknown hydrodynamic coefficients. Rather than using a parameterization with sharp corners, we use softplus functions to parameterize each of the linear components of C_m, $C_{lv,0}$, and $(A_y/D)_c$ as this was found to improve fit. C_{lv} is left as a piecewise linear function so that it can be easily inverted to find A^*. The exact functional forms for each quantity are given in the Appendix A.

Learning Parameters via Optimization

We determine values of the parameters $\mathbf{p} = (p_1, \ldots, p_{11})$ through formulating and minimizing an appropriate error function been theoretical prediction using parameterized hydrodynamic database and given experimental observations.

Take a rigid cylinder of mass m, diameter D and length L, mounted on springs with spring constant k and dashpots with damping constant b in a uniform current of velocity U as an example, its equation of motion is shown as follows,

$$m\frac{d^2y}{dt^2} + b\frac{dy}{dt} + ky = F_l(t), \tag{1}$$

where $F_l(t)$ represents the oscillatory lift force acting from the fluid on the rigid cylinder. When the system achieves a harmonic oscillation assuming an energy balance between fluid and structure, we reach a set of equations for VIV response prediction in a non-dimensional form as follows,

$$V_r(U_r) = U_r\sqrt{\frac{m^* + C_{my}}{m^* + 1}}, \quad A^*(U_r) = \frac{C_{lv}U_r^2}{4\pi^3(m^* + 1)\zeta}, \tag{2}$$

where $V_r = \frac{U}{fD}$ is the true reduced velocity, the inverse of the true reduced frequency $f_r = \frac{fD}{U}$, f is the response frequency, $U_r = \frac{U}{f_n D}$ is reduced velocity, $f_n = \frac{1}{2\pi}\sqrt{\frac{k}{m+\rho_f \forall}}$ is the system natural frequency in the still water, assuming $C_{my} = 1.0$, $m^* = \frac{\rho_s}{\rho_f}$ is the mass ratio, ρ_s is the structural density, ζ is the damping ratio.

In the experiment, we normally do not have knowledge of the true hydrodynamic coefficients. Rather, we have measurements of V_r and A^* as a function of U_r at a given Re. To determine the accuracy of any given parameterization we use Eq. (2) and the parameterization given in the previous section to construct maps $V_r = V_r(U_r, \mathbf{p})$ and $A^* = A^*(U_r, \mathbf{p})$. This requires an inner loop solver to determine U_n for arbitrary V_r. We minimize the residual of the first line of Eq. (2) to find V_r.

$$\hat{V}_r = \underset{V_r}{argmin}\left|V_r - U_r\sqrt{\frac{m^* + C_{my}(V_r; p)}{m^* + 1}}\right|. \tag{3}$$

The amplitude A^* is subsequently found as the unique value which satisfies the second equation in Eq. (2) given the previously found value of V_r and parameterization $\mathbf{p}$. Comparing the observed and predicted reduced velocities and amplitudes, we get the learning objective function as follows,

$$J(\mathbf{p}) = \sum_{j=1}^{n}\frac{(f_{r,j} - \hat{f}_{r,j}(U_r, \mathbf{p}))^2}{\sigma_{f_r}^2} + \frac{(A_j^* - \hat{A}_j^*(U_r, \mathbf{p}))^2}{\sigma_{A^*}^2}, \tag{4}$$

where $\sigma_{f_r}^2$ and $\sigma_{A^*}^2$ are used for normalization.

The Eq. (4) is appended with regularization terms and each p_i is constrained to lie within a physically plausible region, described in the Appendix A. We solve for $\mathbf{p}$ using a randomized coordinate descent algorithm, which was found to perform favorably in comparison to gradient descent and particle swarm methods. Specifically, random perturbations of the current parameterization are taken along a specific axis, and the estimate is adjusted to the sample with the least error before moving to a new axis. The variance of the sampling distribution is reduced as optimization progresses. While heuristic, this algorithm was found to outperform all gradient-based methods, including gradient descent and BFGS, as well as particle swarm methods, simplex methods, and Bayesian optimization.

Similar to the rigid cylinder, the learning of hydrodynamic database of the flexible cylinder VIVs starts with the equation of the motion that describes a flexible cylinder along z-axis between $z = 0$ and $z = L$ with the mass per unit length μ, the structural damping per unit length c, the bending stiffness of EI taut and the tension T, under a time-varying fluid lift force per unit length $f_l(z, t)$ as follows,

$$\mu\frac{\partial^2 y}{\partial t^2} + c\frac{\partial y}{\partial t} - \frac{\partial}{\partial z}(T\frac{\partial y}{\partial z}) + \frac{\partial^2}{\partial z^2}(EI\frac{\partial^2 y}{\partial z^2}) = f_l(z, t). \tag{5}$$

By applying the assumption of the strip theory, the free vibration response of a flexible cylinder in the current can be predicted with the forced vibration constructed hydrodynamic database. When the system

achieves a harmonic oscillation, the problem can be modeled and solved as a nonlinear eigenvalue problem as follows,

$$[-\omega^2(m + C_{my}\forall) + i\omega b]Y - \frac{\partial}{\partial z}(T\frac{\partial Y}{\partial z}) + \frac{\partial^2}{\partial z^2}(EI\frac{\partial^2 Y}{\partial z^2}) = iC_{lv}\frac{\rho_f U^2}{2}D\frac{Y}{|Y|}, \tag{6}$$

where again, C_{my} and C_{lv} are functions of A^* and V_r, which can be found in the hydrodynamic database constructed by the rigid cylinder forced vibration. From eq. (6), we are able to solve $\hat{V}_r(z, U_r^j(z), \mathbf{p})$ and $\hat{A}^*(z, U_r^j(z), \mathbf{p})$ along the span of the flexible cylinder via semi-empirical code VIVA (Triantafyllou *et al*, 1999) using parameterized hydrodynamic database iteratively. Therefore, the objective function of the optimization can be imposed as follows,

$$J(\mathbf{p}) = \sum_{j=1}^{n}(\frac{1}{L}\int |A_j^* - \hat{A}^*(z, U_r^j(z), \mathbf{p})|dz + \lambda|V_r^j - \hat{V}_r(z, U_r^j(z), \mathbf{p})|, \tag{7}$$

where λ is the weight between the model RMSE and the frequency error. Again the parameter $\mathbf{p}$ can be solved via the randomized coordinate descent algorithm used in the rigid cylinder problem.

RESULT AND DISCUSSION

In this section, we demonstrate the application of the proposed methodology to several datasets. We start with the experimental datasets for CF-only rigid cylinder VIVs using force feedback apparatus. Then we show the application of the proposed method to large-scale flexible cylinder experiments in both uniform and linearly shear flow from the Norwegian Deepwater Programme.

Rigid Cylinder Free Vibrations

Using a force feedback laboratory apparatus (Hover *et al*, 1997), CF-only free vibration of a rigid cylinder was studied (Smogeli *et al*, 2003) over a large range of U_r with a fixed $Re = 20,000$. The structural properties were selected as a fixed mass ratio and various damping ratios. The constructed results of C_{lv} and C_{my} are plotted in Fig. 2 (top row). The result shows that learned C_{lv} contour is similar to past CF-Only forced vibration result (Gopalkrishnan, 1993) at a different $Re = 10,000$, and has a narrow positive region around $f_r = 0.16$ with maximum A^* of zero contour line reach $A^* = 1.2$. Meanwhile, the learned C_{my} is shown to have a drastic change from a small negative value to a large positive value at $f_r = 0.15$, similar to the findings in the past forced vibration experiments (Carberry *et al*, 2005).

In Smogeli's experiment, the hydrodynamic coefficients were measured. Therefore, we can compare the experimental measured hydrodynamic coefficient with our learned optimal C_{lv} and C_{my} database and plot the result in Fig. 2 (bottom row, right column). The two sets of data show good linear correlation indicating that the constructed hydrodynamic database using optimal parameters learned from the free vibration matches well with the experimentally measured vortex-induced force on the cylinder model. It is noted in Fig. 2 (bottom row, left column) that the predicted C_{lv} is averagely larger than experimental measured C_{lv}, which may be a result of the experimental error due to the force-feedback setup (Hover *et al*, 1997).

With a good match between experiment measured hydrodynamic coefficient and learned fluid force database, the predicted structural

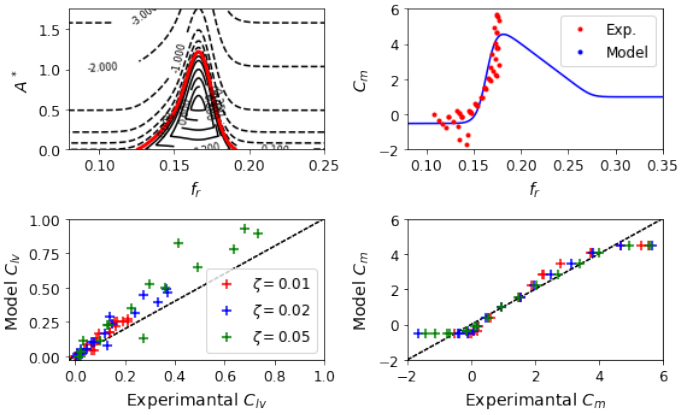

Fig. 2 Learned optimal hydrodynamic database of C_{lv} (left column) and C_{my} (right column). The second row shows the correlation between the experimental measurement and learned parametric model predicted hydrodynamic coefficients.

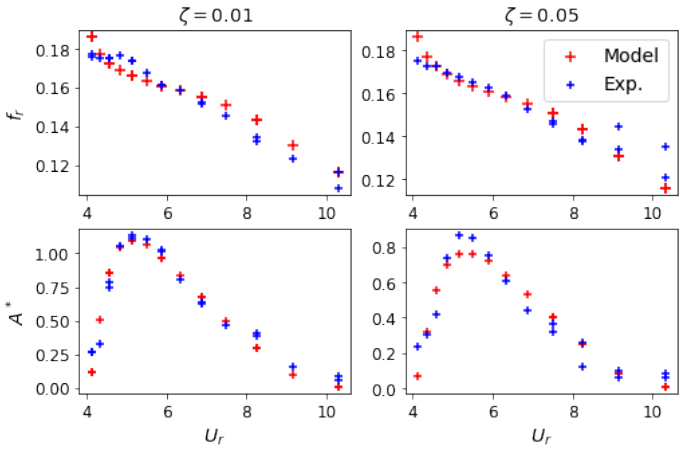

Fig. 3 Comparison between experimental result (blue) and model prediction (red) of frequency (first row) and amplitude (second row) response for different damping ratios: $\zeta = 0.01$ (right column) and $\zeta = 0.05$ (left column).

response is found in good agreement with the experimental result for both displacement and frequency response, shown in Fig. 3. It is noteworthy that with an increase of ζ, the maximum A^* decreases.

Flexible Cylinders Free Vibration

We then test the learning method on the dataset of the Norwegian Deepwater Programme (NDP) large-scale laboratory experiment (Braaten *et al*, 2004) of a 38m uniform flexible riser experiment in both the uniform current and linearly sheared flow with a wide range of different velocities.

To demonstrate the learning process, we plot in Fig. 4 the evolution of the VIVA prediction with the optimized hydrodynamic database over initial guess, first, second and sixth iterations of the $U = 2.0m/s$ case (NDP experiment no. 2182). The left column shows the comparison between the prediction and the experiment. From the result, we can see with the increase of the iteration, the difference between the

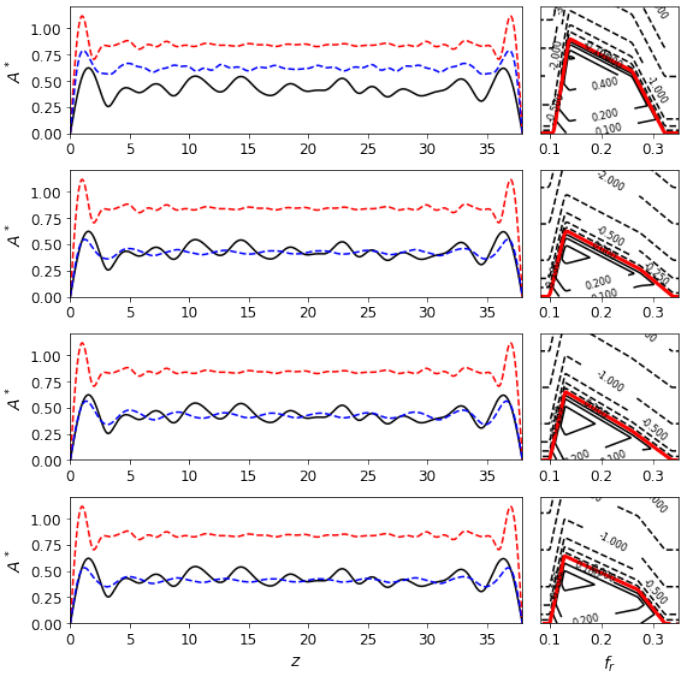

Fig. 4 Evolution of VIVA prediction on the NDP experiment no. 2182 (Uniform velocity $U = 2.0m/s$) at iteration 0 (first row), iteration 2(second row), iteration 4(third row), iteration 6(fourth row). In the left column, the solid black line shows the experimental result; the red dashed line shows the nominal VIVA prediction, and the blue dashed line shows the VIVA prediction with corresponding learned hydrodynamic databases that are shown in the right column for C_{lv}. Additionally, the measured frequency response is 10.23 Hz in the experiment, the nominal VIVA prediction is 12.54Hz, and with the improved hydrodynamic database, the predicted frequency response evolves as 10.71 Hz (iteration 0), 10.62 Hz (iteration 2), 10.56 Hz (iteration 4) and 10.63 Hz (iteration 6).

experiment and VIVA prediction with an optimized hydrodynamic database improves with the increase of the iteration. Furthermore, the last row of the displacement plot shows that with a learned optimal hydrodynamic database (solid blue line), VIVA can provide a better prediction than that using the standard hydrodynamic database (red dashed line), comparing to the experimental result (solid black line). The right column in Fig. 4 plots the corresponding C_{lv} of learned parameters $\mathbf{p}$, and it can be shown that the hydrodynamic database C_{lv} does not vary much at larger iterations, representing a convergence of the learning process. Additionally, the measured frequency response is 10.23 Hz in the experiment, the nominal VIVA prediction is 12.54Hz, and with the improved hydrodynamic database, the predicted frequency response evolves as 10.71 Hz (the initial guess), 10.62 Hz (the second iteration), 10.56 Hz (the fourth iteration) and 10.63 Hz (the sixth iteration). Moreover, we can conclude with the converged optimal hydrodynamic database; VIVA can provide a better prediction on the frequency response.

Using a dataset of cases of uniform flow and cases of linearly sheared flow, we obtained the optimal hydrodynamic database of C_{lv} and C_{my}, shown in the third row of Fig. 5. As an example, no. 2182 cases of

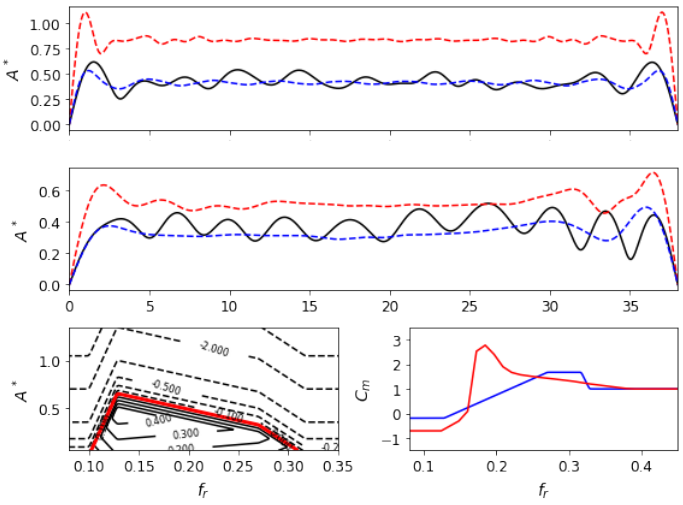

Fig. 5 The sample cases of no. 2182 cases of uniform flow (uniform $U = 2.0m/s$, first row) and no. 2430 cases of linearly sheared flow (maximum $U = 1.5m/s$, second row) are selected to show the difference of the amplitude response among the experimental result (solid black line), nominal VIVA prediction (red dashed line) and VIVA prediction with optimal hydrodynamic database (blue dashed line). The third row shows the learned hydrodynamic database of C_{lv} (left) and C_{my} (right, red line: C_{my} for nominal VIVA and blue line: learned C_{my} based on the NDP experiment).

uniform flow (uniform $U = 2.0m/s$) and no. 2430 cases of linearly sheared flow (maximum $U = 1.5m/s$) are selected out and plotted in the first and second row of Fig. 5. The result can be shown that with an optimally learned hydrodynamic database, the VIVA prediction (solid blue line) has been shown to match better with the experimental result (solid black line) than that of the VIVA prediction using a standard hydrodynamic database (red dashed line).

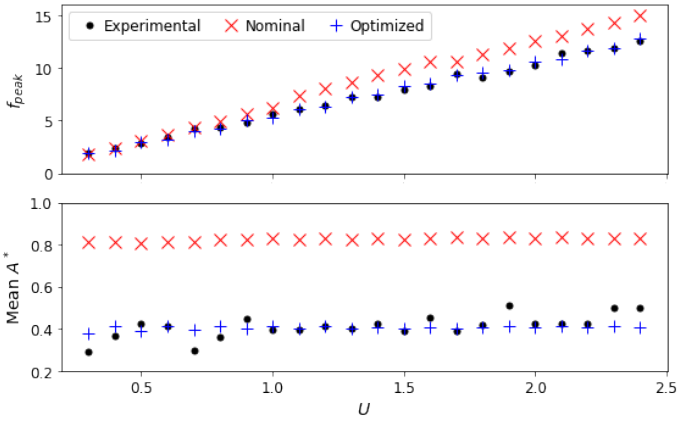

Fig. 6 Comparison of spatial average displacement $\overline{A^*}$ among experimental result (black dot), nominal VIVA prediction (red cross), and VIVA prediction with optimal hydrodynamic database for NDP 38m experiment in uniform flow over different incoming velocity U in a unit of m/s.

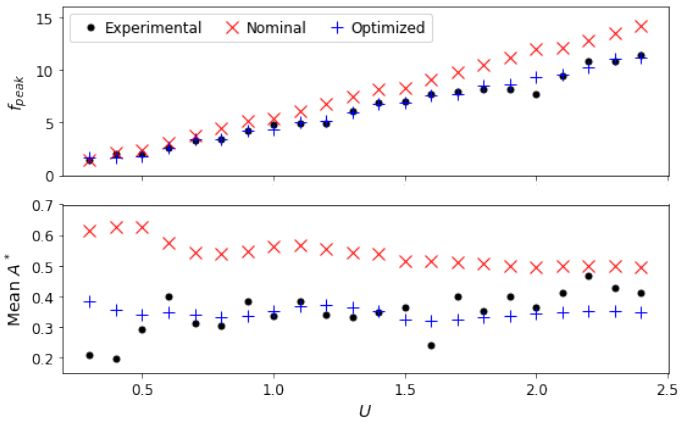

Fig. 7 Comparison of spatial average displacement $\overline{A^*}$ among experimental result (black dot), nominal VIVA prediction (red cross), and VIVA prediction with optimal hydrodynamic database for NDP 38m experiment in linearly sheared flow over different maximum incoming velocity U in a unit of m/s.

In order to summarize the improvements made by the optimally learned hydrodynamic database to the standard one. We plot the peak response frequency f_{peak} and the mean disturbance $\overline{A^*} = \frac{1}{L}\int_0^L A^* dz$ for all velocity cases of the NDP experiment for both uniform (in Fig. 6) and linearly sheared flow (in Fig. 7) cases. The result clearly shows that the prediction with the optimized hydrodynamic database (blue cross) exhibits greater accuracy in both frequency and amplitude prediction than the prediction with the standard database (red star) and that improvements are universal across all velocities.

CONCLUSION

In this work, we present a methodology for determining parametric forms of hydrodynamic databases that can be trained with sparse sensors along a riser's length. The parametric structure of the proposed databases is informed by experiments performed on rigid cylinders forced vibrations. The corresponding parameters can be learned via optimization from the dataset of both rigid and flexible cylinders VIVs. We show that the proposed method yields more accurate predictions for VIV amplitude and frequency both in rigid and flexible cylinder experiments.

ACKNOWLEDGEMENTS

We gratefully acknowledge support from the DigiMaR Consortium, consisting of ABS, ExxonMobil, Petrobras, SAIPEM, Shell, and Subsea 7.

REFERENCES

Aronsen, K. H. (2007). "An experimental investigation of in-line and combined in-line and cross-flow vortex induced vibrations", PhD thesis, Norwegian University of Science and Technology.

Braaten, H., and Lie, H. (2004). "NDP riser high mode VIV tests", Norwegian Marine Technology Research Institute, Technical Report(512394.00), p. 01.

Carberry, J., Sheridan, J., and Rockwell, D. (2005). "Controlled oscillations of a cylinder: forces and wake modes", *Journal of Fluid Mechanics.*, Vol 538, pp. 31–69.

Chang, C. C. J., Kumar, R. A., and Bernitsas, M. M. (2011). "Viv and galloping of single circular cylinder with surface roughness at Re from 3.0*10^4 to 1.2*10^5", *Ocean Engineering.*, Vol 38(16), pp. 1713–1732.

Chen, Y., Fu, S. X., Xu, Y. W., Zhou, Q., and Fan, D. (2013). "Hydrodynamic characters of a near-wall circular cylinder oscillating in cross flow direction in steady current", *Acta Physica Sinica.*, Vol 62(6), p. 064701.

Dahl, J. (2008). "Vortex-induced vibration of a circular cylinder with combined in-line and cross-flow motion", PhD thesis, Massachusetts Institute of Technology.

Fan, D., Wang, Z., Triantafyllou, M. S., and Karniadakis, G. E. (2019). "Mapping the properties of the vortex-induced vibrations of flexible cylinders in uniform oncoming flow", *Journal of Fluid Mechanics.*, Vol 881, 815-858.

Fan, D., Jodin, G., Consi, T. R., Bonfiglio, L., Ma, Y., Keyes, L. R., Karniadakis G. E., and Triantafyllou, M. S. (2019). "A robotic intelligent towing tank for learning complex fluid-structure dynamics", *Science Robotics.*, Vol 4(36).

Fan, D., and Triantafyllou, M. S. (2020). "Vortex induced vibration of riser with low span to diameter ratio buoyancy modules", In The 27th International Ocean and Polar Engineering Conference, International Society of Offshore and Polar Engineers.

Gabbai, R., and Benaroya, H. (2005). "An overview of modeling and experiments of vortex-induced vibration of circular cylinders", *Journal of Sound and Vibration.*, Vol 282(3-5), pp. 575–616.

Gopalkrishnan, R. (1993). "Vortex-induced forces on oscillating bluff cylinders", PhD thesis, Massachusetts Institute of Technology.

Han, Q., Ma, Y., Xu, W., Fan, D., and Wang, E. (2018). "Hydrodynamic characteristics of an inclined slender flexible cylinder subjected to vortex-induced vibration", *International Journal of Mechanical Sciences.*, Vol 148, pp. 352–365.

Hover, F., Miller, S., and Triantafyllou, M. (1997. "Vortex-induced vibration of marine cables: experiments using force feedback", *Journal of Fluids and Structures.*, Vol 11(3), pp. 307–326.

Larsen, C. M., Vikestad, K., Yttervik, R. (2001). "Vivana theory manual", Marintek, Trondheim, Norway.

Lin, K., Fan, D., and Wang, J. (2020). "Dynamic response and hydrodynamic coefficients of a cylinder oscillating in crossflow with an upstream wake interference", *Ocean Engineering.*, Vol 209, p. 107520.

Mukundan, H. (2008). "Vortex-induced vibration of marine risers: motion and force reconstruction from field and experimental data", PhD thesis, Massachusetts Institute of Technology.

Roveri, F. E., and Vandiver, J. K. (2001). "Using shear7 for assessment of fatigue damage caused by current induced vibrations", In Proc. 20th OMAE Conf, pp. 3–8.

REFERENCES

Smogeli, O. N., Hover, F. S., and Triantafyllou, M. S. (2003). "Force-feedback control in VIV experiments", *International Conference on Offshore Mechanics and Arctic Engineering.*, Vol 36835, pp. 685–695.

Triantafyllou, M., Triantafyllou, G., Tein, Y. S., and Ambrose, B. D. (1999). "Pragmatic riser viv analysis", In Offshore technology conference, Offshore Technology Conference.

Wang, J., Fan, D., and Lin, K. (2020). "A review on flowinduced vibration of offshore circular cylinders", *Journal of Hydrodynamics.*, Vol 32(3), pp. 415–440.

Wang, Z., Fan, D., Triantafyllou, M. S., and Karniadakis, G. E. (2021). "A large-eddy simulation study on the similarity between free vibrations of a flexible cylinder and forced vibrations of a rigid cylinder", *Journal of Fluids and Structures.*, Vol 101, p. 103223.

Williamson, C. H. K. (1996). "Vortex dynamics in the cylinder wake", *Annu. Rev. Fluid Mech.*, Vol 28(1), pp. 477– 539.

Williamson, C. H. K., and Govardhan, R. (2004). "Vortex-induced vibrations", *Annu. Rev. Fluid Mech.*, Vol 36, pp. 413–455.

Xu, Y., Fu, S., Chen, Y., Zhong, Q., and Fan, D. (2013). "Experimental investigation on vortex induced forces of oscillating cylinder at high reynolds number", *Ocean Systems Engineering.*, Vol 3(3), pp. 167–180.

Appendix A: Parametric Hydrodynamic Databases

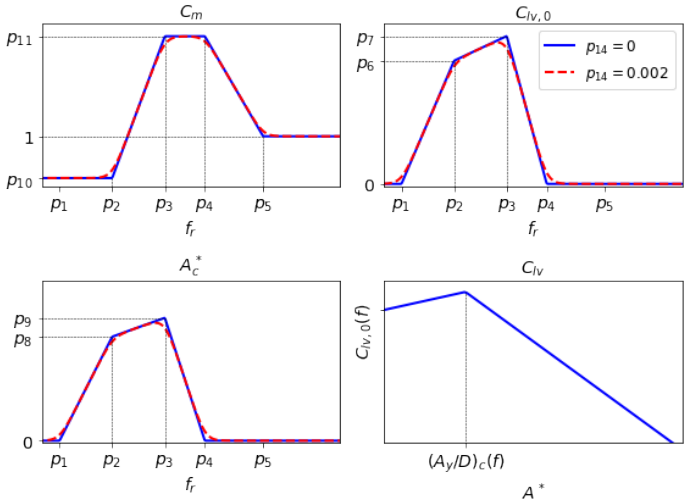

Fig. 8 Parameteric model for the hydrodynamic database.

The hydrodynamic coefficients are defined as functions of reduced frequency and amplitude using a fourteen dimensional parametric representation. The effect of the first thirteen of these parameters is shown in Fig. 8 with the fourteenth parameter acting as a smoothing factor for transitions between linear components. Descriptions of each parameter are given in table 1. Note that in the non-smoothed case the parameters $p_6 - p_9$ define the exact values of $C_{lv,0}$ and A_c^* at frequencies p_2 and p_3 but when we use a smoothed representation this will no longer be the case. The smoothed forms of C_m, $C_{lv,0}$, and A_c^* are given in terms of the soft-plus function which is defined by,

$$s_w(f) = w\ \log(1 + exp(f/w)) \tag{8}$$

Table 1 Description of parameters for hydrodynamic coefficients.

$p_1 - p_5$	f_r used for C_m, $C_{lv,0}$, and A_c^*.
p_6, p_7	Parameters for values of $C_{lv,0}$ at p_2, p_3.
p_8, p_9	Parameters for values of A_c^* at p_2, p_3.
p_{10}, p_{11}	Values of constant sections of C_m curve.
p_{12}	Slope of C_{lv} w.r.t. A^* for $A^* < A_c^*$
p_{13}	Slope of C_{lv} w.r.t. A^* for $A^* > A_c^*$
p_{14}	Characteristic width of softplus function.

where w is a learned length scale. As $w \to 0$ the soft-plus function converges uniformly to the rectified linear unit, allowing for smooth approximation of piece wise linear functions. The added mass coefficient is given by,

$$\begin{aligned} C_m = {} & p_{10} + m_1(s_{p_{14}}(f - f_2) - s_{p_{14}}(f - f_3)) \\ & + m_2(s_{p_{14}}(f - f_4) - s_{p_{14}}(f - f_5)) \end{aligned} \tag{9}$$

where,

$$m_1 = \frac{p_{11} - p_{10}}{p_3 - p_2} \qquad \text{and} \qquad m_2 = \frac{1 - p_{11}}{p_5 - p_4}. \tag{10}$$

The values of $C_{lv,0}$ and A_c^* are given by,

$$\begin{aligned} C_{lv,0} = {} & m_3(s_{p_{14}}(f - f_1) - s_{p_{14}}(f - f_2)) + m_4(s_{p_{14}}(f - f_2) \\ & - s_{p_{14}}(f - f_3)) + m_5(s_w(f - f_3) - s_{p_{14}}(f - f_4)) \end{aligned} \tag{11}$$

and

$$\begin{aligned} A_c^* = {} & m_6(s_{p_{14}}(f - f_1) - s_{p_{14}}(f - f_2)) + m_7(s_{p_{14}}(f - f_2) \\ & - s_{p_{14}}(f - f_3)) + m_8(s_{p_{14}}(f - f_3) - s_{p_{14}}(f - f_4)), \end{aligned} \tag{12}$$

where

$$\begin{aligned} m_3 &= \frac{p_6}{p_2 - p_1}, & m_4 &= \frac{p_7 - p_6}{p_3 - p_2}, & m_5 &= \frac{-p_7}{p_4 - p_3} \\ m_6 &= \frac{p_8}{p_2 - p_1}, & m_7 &= \frac{p_9 - p_8}{p_3 - p_2}, & m_8 &= \frac{-p_9}{p_4 - p_3} \end{aligned} \tag{13}$$

Finally, C_{lv} is given by,

$$C_{lv} = \begin{cases} C_{lv,0} + A^* p_{12}, & \text{if } A^* \le A_c^* \\ C_{lv} = C_{lv,0} + A_c^* p_{12} - (A^* - A_c^*) p_{13}, & \text{if } A^* > A_c^* \end{cases} \tag{14}$$

Each variable is bounded based on the intervals described in Tab. 2. Open boundaries are enforced through fitting the transformed variables $q_i = \sigma^{-1}((p_i - p_{min})/(p_{max} - p_{min}))$ where p_{min} andp_{max} are the bounds for the given parameter and σ is the standard sigmoid function.

Table 2 Bounds of parameters for hydrodynamic coefficients.

p_1	$(0.08, 0.245)$
p_n, $n = 2, 3, 4, 5$	$(p_{n-1}, 0.35)$
$p_6 - p_7$	$(0, 0.25)$
$p_8 - p_9$	$(0, 2)$
p_{10}	$(-2, 1)/(-2, 0)$
p_{11}	$(1, 10)/(1, 5)$
p_{12}	$(0.1, 5)$
p_{13}	$(1, 5)$
p_{14}	$(0, 0.005)$